Current Biology 24, 2888–2898, December 15, 2014 ©2014 Elsevier Ltd All rights reserved http://dx.doi.org/10.1016/j.cub.2014.10.028

Article

Coincidence Detection of Single-Photon Responses in the Inner Retina at the Sensitivity Limit of Vision

Petri Ala-Laurila[1,2,*] and Fred Rieke[2]
[1]Department of Biosciences, University of Helsinki, P.O. Box 65, 00014 Helsinki, Finland
[2]Howard Hughes Medical Institute and Department of Physiology and Biophysics, University of Washington, Seattle, WA 98195, USA

Summary

Background: Vision in starlight relies on our ability to detect single absorbed photons. Indeed, the sensitivity of dark-adapted vision approaches limits set by the quantal nature of light. This sensitivity requires neural mechanisms that selectively transmit quantal responses and suppress noise. Such mechanisms face an inevitable tradeoff because signal and noise cannot be perfectly separated, and rejecting noise also means rejecting signal.
Results: We report measurements of single-photon responses in the output signals of the primate retina. We find that visual signals arising from a few absorbed photons are read out fundamentally differently by primate On and Off parasol ganglion cells, key retinal output neurons. Off parasol cells respond linearly to near-threshold flashes, retaining sensitivity to each absorbed photon but maintaining a high level of noise. On parasol cells respond nonlinearly due to thresholding of their excitatory synaptic inputs. This nonlinearity reduces neural noise but also limits information about single-photon absorptions.
Conclusions: The long-standing idea that information about each photon absorption is available for behavior at the sensitivity limit of vision is not universally true across retinal outputs. More generally, our work shows how a neural circuit balances the competing needs for sensitivity and noise rejection.

Introduction

Sensory receptors exhibit impressive sensitivity: auditory hair cells detect displacements of subatomic dimensions [1, 2], pheromone receptors respond to single molecules [3], and rod photoreceptors detect single photons [4]. The neural circuits that read out the receptor responses inevitably add noise that threatens to limit sensory performance. High initial amplification can mitigate the effect of such readout noise, but this strategy alone may not be sufficient when the signals of interest are carried by a small fraction of the receptors, i.e., are sparse. Under these conditions, convergence of multiple inputs on downstream cells raises a general problem: how to separate the sparse signals of interest from the noise present in all the inputs.

Seeing in starlight exemplifies this problem because photons arrive rarely at individual rod photoreceptors. Visually guided behavior under these conditions relies on detecting signals generated by <0.1% of the rods in the presence of noise generated by all the rods (reviewed in [5]). Linear integration (i.e., averaging) of rod signals under these conditions would be disastrous for visual sensitivity; instead, reliable readout of the rod signals requires separation of single-photon responses from noise—e.g., by thresholding—prior to integration [6, 7]. Indeed, rod signals are thresholded at the first synapse in the rod bipolar pathway [8–10], a dedicated retinal circuit that processes mammalian rod signals at low light levels [11–16].

A near-identical problem recurs at later stages of retinal processing. Responses to single absorbed photons remain sparse throughout many of the neurons that comprise the retinal readout of the rod signals. Meanwhile, synaptic and cellular processes in these neurons necessarily add noise that threatens to obscure the sparse responses to single absorbed photons. This added noise raises the possibility that additional thresholding steps at key sites of convergence within the retinal circuitry serve to reduce noise. But such thresholding will reject both noise and a fraction of the single-photon responses. This tradeoff is the common problem of balancing false positives (noise-driven responses) and false negatives (missed single-photon responses) encountered in any near-threshold discrimination task. This balance relates to the decades-old problem of whether information about each absorbed photon is available for perceptual decisions, or instead if neural mechanisms impose a threshold below which information is unavailable (reviewed by [17]). Our aims here were to understand how mechanisms in the primate retina balance noise rejection and signal retention at absolute visual threshold and to determine whether different parallel retinal outputs strike the same balance.

Results

On and Off Parasol Ganglion Cells Both Have High Sensitivity but Different Coding Strategies at Detection Threshold

To characterize retinal output signals of direct relevance for human behavior, we recorded the electrical responses of dark-adapted primate ganglion cells to flashes near behavioral threshold. We emphasized On and Off parasol (magnocellular-projecting) ganglion cells, which most likely contribute to absolute behavioral sensitivity since they receive abundant rod input [18, 19] and provide information about subtle changes in contrast to appropriate central targets [20].

Spontaneous and light-evoked responses of On and Off parasol cells differed markedly. On parasol cells generated few spontaneous spikes (Figure 1A; dark firing rate 0.48 ± 0.09 Hz, mean ± SEM, n = 59), whereas Off parasol cells had a substantial spontaneous firing rate (Figure 1B; dark firing rate 19.9 ± 3.2 Hz, mean ± SEM, n = 7). The low dark activity of On parasol cells was surprising, given that 10–20 spontaneous photon-like noise events occur every second in the collection of ~4,000 rods providing (indirect) input to the recorded cells (eccentricity >20°; see the Experimental Procedures; [5, 6, 21]); assuming linear integration and the generation of approximately one spike per photoisomerization (see below and [22, 23]), these spontaneous events should produce dark firing rates of 10–20 spikes/s. Substantial dark activity

*Correspondence: petri.ala-laurila@helsinki.fi

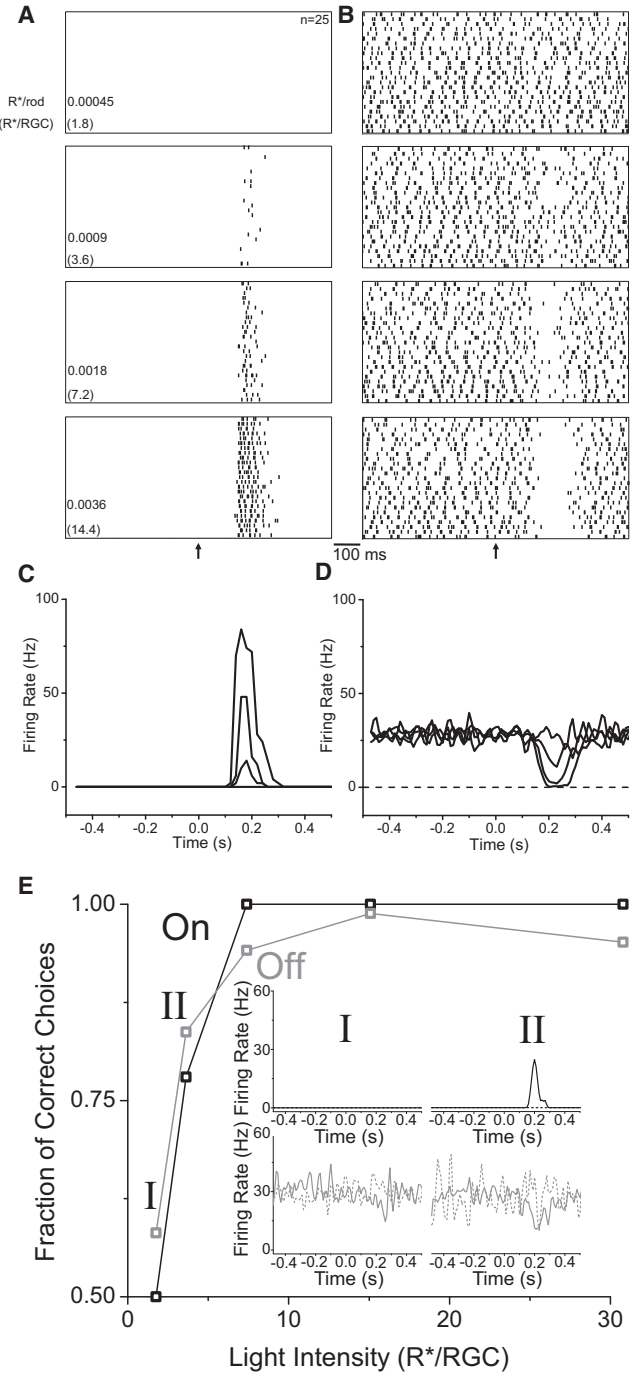

Figure 1. On and Off Parasol Ganglion Cells Encode Weak Flashes Differently

(A) On parasol ganglion cell spike responses to dim flashes delivered at the time of the arrow. Each box shows 25 trials with flashes of constant nominal intensity as indicated in the lower left corner.

(B) Off parasol ganglion cell (neighboring cell in the same preparation as the cell in (A) spike responses to the same flash strengths as in (A).

(C) On parasol cell mean firing rates (PSTH; 10 ms time bin) for the same cell and flash strengths as in (A).

(D) Off parasol cell mean firing rates for the same cell and flash strengths as in (B).

(E) Two-alternative forced-choice task for the same On (black) and Off (gray) parasol cells as shown in (A)–(D). The inset shows the average of all correct choices (continuous line) and incorrect choices (dashed line) for On (black; top) and Off (gray; bottom) parasols at the two lowest light intensities indicated by roman numerals (I and II) both in the main panel and inset.

has been observed in in vivo recordings from On center ganglion cells in anesthetized cats [22, 23] and attributed to linear summation of spontaneous photon-like events (reviewed by [17]). The near silence of dark-adapted On parasol cells is inconsistent with this linear model.

Both On and Off parasol cells generated discernible responses to flashes that produced approximately three to four absorbed photons within the entire receptive field of the ganglion cell (i.e., 3–4 isomerizations per parasol ganglion cell [R*/RGC]; Figures 1A–1D). Responses of On parasol cells, when present, were easily identified due to the low spontaneous firing rates of the cells (Figure 1A). Responses of Off parasol cells could be masked by gaps in the ongoing spontaneous activity (Figure 1B). Both cell types responded strongly to flashes producing ~15 R*/RGC, with On cells generating five to ten spikes and Off cells completely suppressing their spontaneous firing.

We used a two-interval forced-choice analysis to explore how the differences in firing properties illustrated in Figures 1A–1D affected sensitivity (see the Experimental Procedures and [24, 25]). Discrimination was based on spike responses during the intervals before and after the flash. The task was to determine which of the two responses was more likely elicited by the flash. Responses of both On and Off parasol cells permitted better-than-chance detection of flashes producing 3–4 R*/RGC (Figure 1E). Off parasol cells were generally more sensitive to the dimmest flashes and less sensitive to the brightest flashes than On parasol cells. More strikingly, the responses that were incorrectly discriminated differed considerably. As the flash intensity increased, Off parasol cells showed a gradually increasing difference between the correct (solid gray traces in the Figure 1E inset) and incorrect (dashed gray traces in the Figure 1E inset) choices. This difference was already present on average at the lowest flash strengths (I and II in Figure 1E). Incorrect discrimination was dominated by random gaps in firing due to noise. On parasol cells either responded robustly or failed to respond altogether (see the solid and dashed black traces in the Figure 1E inset). Thus incorrect discrimination for On parasol responses was dominated by trials in which the cell failed to respond.

On, but Not Off, Parasol Ganglion Cells Nonlinearly Integrate Single-Photon Responses in the Dark

Competing models for absolute visual sensitivity assume either that ganglion cells linearly integrate responses of rods that absorb photons or that instead ganglion cells respond only to multiple absorbed photons (reviewed by [17]). As described below, the answer to this question depends on cell type in the primate retina: Off parasol cells integrated photon absorptions linearly or near linearly, whereas On parasol cells exhibited strongly nonlinear integration.

Figure 2A shows the dependence of firing rate on flash strength for example On and Off parasol ganglion cells. Linear integration would produce a slope of one on this log-log plot (dashed line). The decrease in firing rate of the Off parasol cell to flashes producing <10 R*/RGC follows this linear expectation, whereas for brighter flashes the response saturates as firing is completely suppressed. On parasol responses increased more steeply with flash strength; the slope of near two indicates that the responses grew approximately as the square of the flash strength. The difference in the dependence of On and Off parasol responses on flash strength held across recorded cells (Figure 2A, inset).

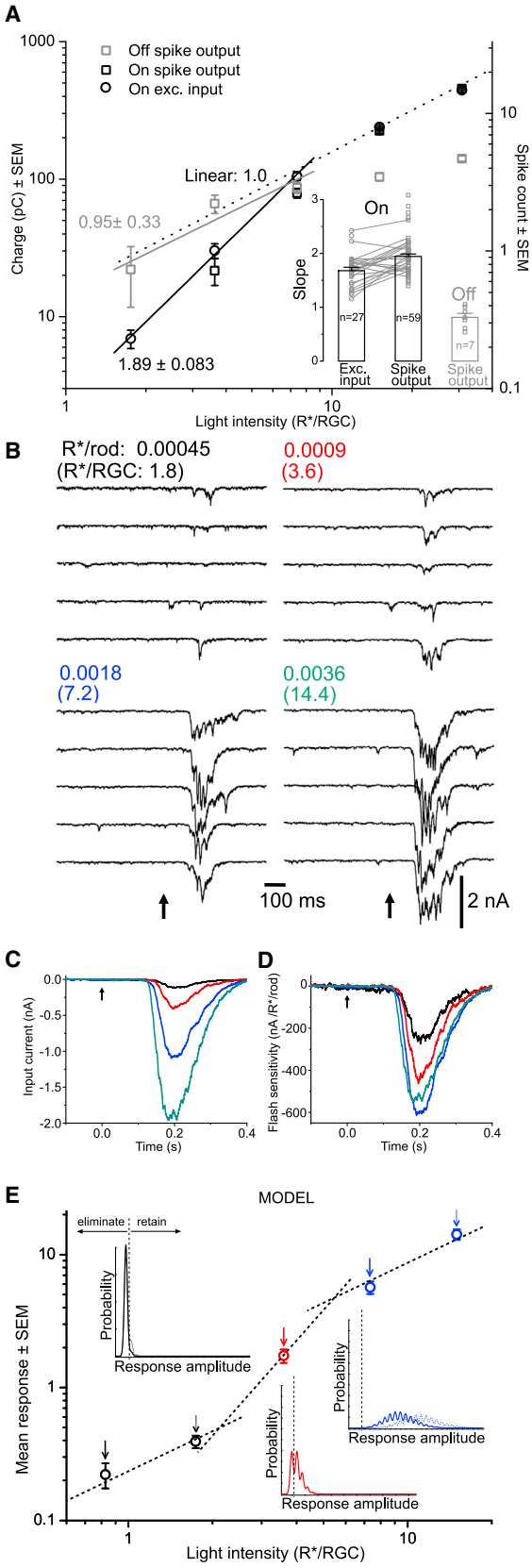

Figure 2. On but Not Off Parasol Ganglion Cells Integrate Single-Photon Responses Nonlinearly

(A) Response amplitude (increase in mean firing rate or mean excitatory current) as a function of flash strength for On parasol cells (black symbols) and for Off parasol cells (decrease in mean firing rate; gray symbols). The cells are the same example cells as in Figure 1. The dashed line shows the expectation for linear integration. Inset: collected data on the slope of the stimulus-response relation (mean ± SEM) in the nonlinear region (On parasols;black bar graphs) and in the same domain in Off parasols (gray bar graph). Slopes were determined over the range of flash strengths where flash sensitivity (response per photoisomerization, as shown in D, grew from 5% to 95% of maximum for On parasols). Symbols connected by lines are from the same cells.

(B) On parasol excitatory synaptic inputs to the same cell and flash strengths as in Figure 1A.

(C) Mean excitatory currents (115 trials at each flash strength) for the same cell and flash strengths.

(D) Sensitivity of input currents—i.e., response divided by flash strength.

(E) A simple thresholding model can explain the shape of the stimulus-response relation. Data points show integrated excitatory synaptic inputs (mean ± SEM) for seven On parasol cells that were probed using the weakest flashes producing <1 R*/RGC. The nonlinear region of the stimulus-response relation occurs where changes in flash strength shift structure in the response distribution from below threshold to above threshold (e.g., the red data point). Peaks in the modeled response distributions are due to discrete photon counts arising from Poisson distribution of the absorbed photons. The spread in the peak of the modeled distributions comes from additive Gaussian noise.

The nonlinearity apparent in the responses of On parasol cells is consistent with a threshold that causes the average response to two absorbed photons to be larger than twice the average single-photon response. Such a threshold could eliminate noise generated from spontaneous rhodopsin activation or within the retinal circuitry and hence explain the low spontaneous firing rate of On parasol cells. We investigated the origin of this nonlinearity since it was unexpected from past work on mammalian ganglion cells [22, 23] and because we were interested in the impact of nonlinear integration on how rod responses to single photons were encoded in the retinal output.

The nonlinear responses of On parasol cells could originate within the retinal circuits that control synaptic inputs to the cell and/or from mechanisms intrinsic to the ganglion cell such as spike generation. To distinguish between these possibilities, we measured the excitatory synaptic inputs to On parasol cells by voltage-clamping the cells at the reversal potential (~−70 mV) for inhibitory synaptic input. Consistent with their low spontaneous firing rates, On parasol cells received minimal spontaneous excitatory synaptic input in the dark (Figure 2B). This absence of spontaneous input, like the absence of spontaneous spikes, indicates that noise due to spontaneous activation of rhodopsin is largely unable to traverse On retinal circuits and modulate the ganglion cell response.

We divided the average On parasol responses to dim flashes (Figure 2C) by the flash strength to estimate the sensitivity, or response per absorbed photon (Figure 2D). Sensitivity of the excitatory synaptic inputs increased with increasing flash strength; as expected, this increased sensitivity resulted in a greater-than-linear dependence of the response amplitude on flash strength (Figure 2A; slope ~2). The nonlinear dependence of excitatory input on flash strength closely mirrored that of the spike output (Figure 2A, inset; lines connect cells in which both spikes and excitatory inputs were measured).

The nonlinearities of On parasol responses are consistent with a thresholding nonlinearity that eliminates or suppresses many single-photon responses. Such a nonlinearity predicts three distinct regions of the stimulus-response relation (Figure 2E). (1) Very low flash strengths rarely produce more than

one absorbed photon within the collection of rods pooled prior to the threshold, and only large responses to single photons or responses that occur together with large noise fluctuations exceed threshold. Increasing the flash strength increases the probability that a single photon is absorbed within the rod pool, but the probability that two photons are absorbed remains negligible. Thus, the threshold operates effectively only on responses to single photons. As a result, the fraction of responses eliminated by the threshold is nearly independent of flash strength, and the stimulus-response relation is linear (black symbols and distributions in Figure 2E). (2) For somewhat brighter flashes, increases in flash strength produce sizable increases in the probability that two photons are absorbed within the rod pool (red symbol and distribution in Figure 2E). These responses produce a supralinear stimulus-response relation since they exceed threshold and are not eliminated by the thresholding mechanism. Doubling of the flash strength in this intensity range causes on average more than a doubling of the response. (3) For flash strengths at which the mean response is considerably larger than threshold, few or no responses are eliminated. The stimulus-response relation is again linear, since increasing the flash strength does not change the fraction of responses eliminated by the threshold (see the blue symbols and distributions in Figure 2E). The transition between the two different linear regions (regions 1 and 3) of the stimulus-response relation depends on the height of the threshold relative to the single-photon response and the number of rod signals pooled at the location of the threshold.

The experiments illustrated in Figures 1 and 2 highlight a nonlinear mechanism controlling signal and noise in the synaptic inputs and spike outputs of On, but not Off, parasol ganglion cells. The nonlinearity is engaged by flashes producing absorbed photons in 0.0005%–0.002% of the rods. Since the nonlinearity is present in the On parasol excitatory synaptic inputs, it must be largely located in the retinal circuitry that conveys rod signals to On parasol cells, rather than in the ganglion cell itself. Below, we investigate the functional consequences and the location of the nonlinearity.

Impact of Nonlinearity on Encoding Sparse Input Signals

How does the nonlinearity in the On parasol responses impact the fidelity with which the cells encode sparse visual signals? Answering this question requires estimating signal and noise in the On parasol responses with and without the nonlinearity.

The model in Figure 2E predicts that the impact of the nonlinearity will be minimized by background light that produces sufficient mean activity to shift most of the responses to amplitudes above the threshold (see Figure 3A, top). Indeed, in the presence of backgrounds producing at least 0.008 R*/rod/s, excitatory inputs and spike outputs of On parasol cells depended near linearly on flash strength (Figures 3A and 3B). Such backgrounds increase the rate of photon-like events in the rods ~2-fold compared to those arising from spontaneous rhodopsin activation alone (0.003 to 0.006 R*/rod/s) [5, 6]. With linear integration, these backgrounds would produce at most a 2- to 3-fold increase in the variance of a ganglion cell's synaptic inputs and spike outputs; the increase in variance would be even smaller if noise from sources other than rhodopsin activation is substantial. Instead, the variance increased 20-fold (excitatory inputs) to 60-fold (spike counts) (Figures 3C and 3D). This strong dependence of noise on background is further evidence for a nonlinearity that suppresses noise in darkness.

To estimate how much nonlinear integration reduced dark noise, we extrapolated the variance from backgrounds in which the stimulus-response relation is linear (green line in Figure 3A) to darkness (dashed line in Figure 3C; see the Figure 3 legend). This extrapolation indicated that the nonlinearity suppressed noise 5-fold (excitatory inputs) to 20-fold (spikes) (Figure 3D, gray symbols and black bars). Such noise suppression comes at the cost of suppressing responses to small numbers of absorbed photons (Figure 2E). Two approaches to estimating the loss in signal yielded similar results. First, we used the maximal flash sensitivity in darkness (flashes producing ~10 R*/RGC; see Figure 2D) to predict the amplitudes of responses to weaker flashes assuming linearity. We then compared these predicted linear responses to those actually observed to estimate how much the nonlinearity suppressed the measured responses. Second, we compared the sensitivity of (linear) average responses measured in the presence of a weak background (see the green symbols in Figure 3A) to responses to the same flashes in the absence of the background.

We used these estimates of the signal and noise without the nonlinearity to evaluate its impact on the fidelity of encoding of sparse signals. Thus we compared the measured dark signal-to-noise ratio (flash sensitivity divided by the standard deviation of the noise) with that estimated for linear responses. For flashes producing $\geq$4 R*/RGC, the decrease in noise due to the nonlinearity was greater than the decrease in signal; as a consequence, the nonlinearity improved the signal-to-noise ratio in the dark by a factor of 2–4 compared to a linear readout (Figure 3E). For flashes producing $\leq$2 R*/RGC, the decrease in signal was similar to or slightly greater than the decrease in noise. As a consequence, linear readouts had equal or higher signal-to-noise ratios compared to nonlinear readouts for the lowest flash strengths. This result is consistent with the differences in discrimination in Figure 1E, where responses of Off parasol cells allowed better discrimination performance at the lowest flash strengths, but On parasol responses provided better discrimination for flashes producing >4–5 R*/RGC.

Nonlinearity Is Located at the Primary Excitatory Synapse onto the Ganglion Cell

The light levels at which nonlinear integration is apparent constrain the potential locations within the retina. Since signals producing as few as 1–2 R* per thousand rods are integrated nonlinearly, the nonlinearity must arise at a location receiving converging input from at least 500–1,000 rods (Figure 4A). This requirement precludes the known nonlinearity at the synapse between rod photoreceptors and rod bipolar cells, which operates on signals from individual rods at flash strengths ~1,000-fold higher (see Figure S1 available online). Rod convergence has been studied most thoroughly in cat retina, where each AII amacrine cell pools signals from ~300–500 rods [26, 27]; synaptic terminals of On cone bipolar cells pool from a similar number of rods when signals traverse the retina through the rod bipolar pathway since they effectively inherit the rod convergence present in the AII amacrine responses [26]. Assuming similar levels of convergence in primate retina, the nonlinearity must be located between the inputs to AII amacrine cells and inputs to On parasol ganglion cells. Our recorded On parasol ganglion cells pool signals from ~4,000 rods [21].

Two experiments identified the cone bipolar output synapse as the location of the nonlinearity (Figure 4). First, just as observed for spike outputs (Figure 2A), flashes that produced

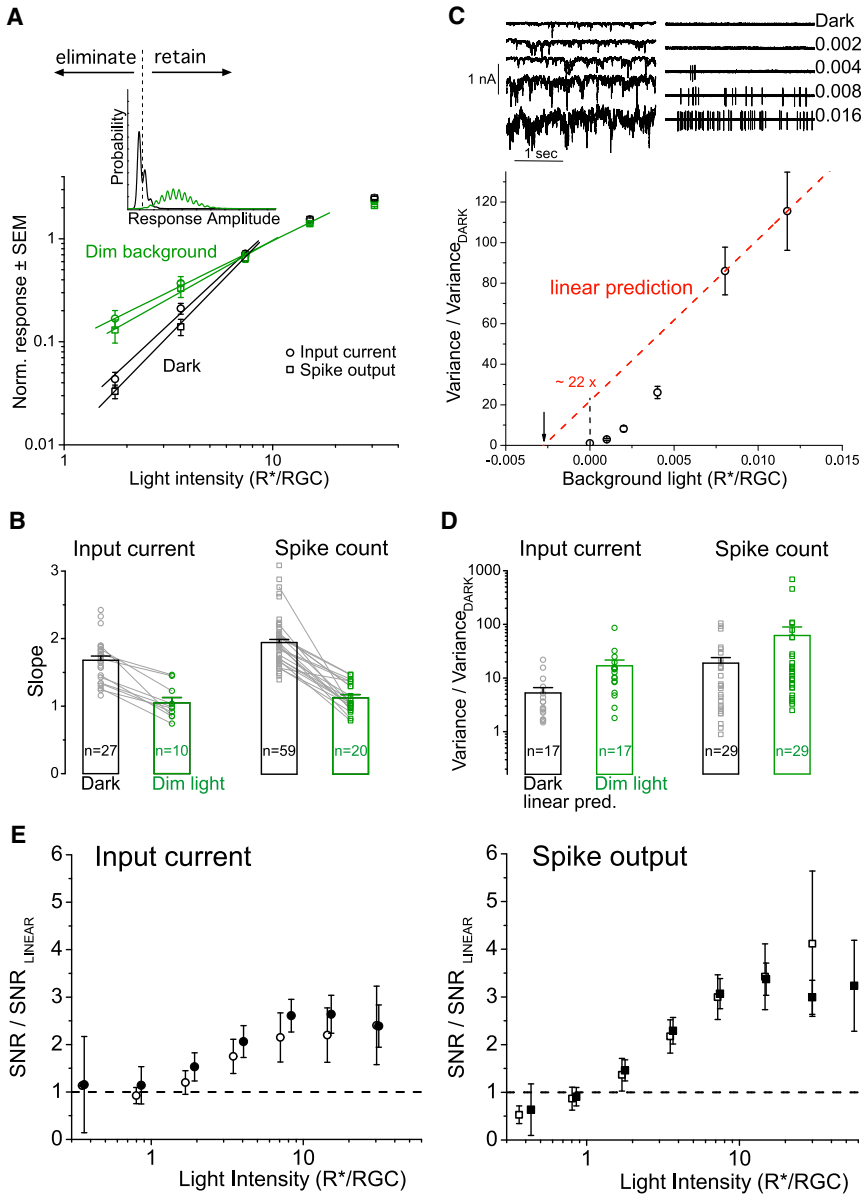

Figure 3. Dim Backgrounds Eliminate the Nonlinearity in On Parasol Responses

(A) Stimulus-response relations for spike responses and excitatory synaptic inputs in darkness (black lines and symbols) and in the presence of a dim background (green lines and symbols) (different cells were used for spike and input current measurements). A simple threshold model (inset) predicts relief of the nonlinearity by a background light that shifts the response distribution above the threshold.

(B) Summary of effect of background on the slope of the stimulus-response relation.

(C) The dependence of noise variance on background light in an example On parasol cell. The upper part shows example traces of current noise (left) and spiking noise (right) in the same cell at the same light levels (background intensities are indicated in units of R*/rod/s). The current noise traces were matched filtered by the cell's impulse response prior variance estimation to focus on the most critical noise component (see the lower part of the plot). The dashed line plots the expectation if the variance increased linearly with increasing Poisson fluctuations due to the background. The x axis intercept of this line provides an estimate of the dark noise (equivalent to 0.0027 R*/rod/s). The steep decrease in the variance measured at the lowest backgrounds reflects suppression of noise due to the nonlinear threshold.

(D) Collected data on the ratio of the linearly predicted variance to the measured variance in darkness (gray symbols and black bars) and the variance measured under one dim background intensity, 0.008 R*/rod/s, versus that in darkness (green symbols and bars). In a subpopulation of the cells, we measured the variance only in darkness and at one background (0.008 R*/rod/s). In such cases, the extrapolation was based on the variance measured at 0.008 R*/rod/s and the x axis intercept was fixed to −0.003 R*/rod/s. Bar graphs show mean ± SEM: Var_{DIM}/Var_{DARK} = 62 ± 28 (spikes), 17 ± 5 (excitatory inputs); $Var^{LIN}_{DARK}/Var_{DARK}$ = 19 ± 5 (spikes), 5.3 ± 1.4 (excitatory inputs).

(E) Signal-to-noise ratio (mean response per photoisomerization / SD of noise) as a function of flash strength. The measured signal-to-noise ratio has been scaled by that expected for a linear system, assuming the maximum flash sensitivity (cf. Figure 2D) and noise as determined in (C) (dashed line) by extrapolation of the measured variance to darkness from backgrounds that relieve the nonlinearity. Open symbols show the signal-to-noise ratio (SNR; mean ± SEM) for excitatory inputs (n = 10 cells) and spike output (n = 24) for On parasol cells in which signal and noise were measured in the same cells. Closed symbols show SNR estimates for On parasol cells in which noise (n = 17 cells, excitatory inputs; n = 29, spike output) and signals (n = 26, excitatory inputs; n = 58, spike output) were measured from different cells.

nonlinear excitatory inputs to On parasol cells produced linear excitatory inputs to Off parasol cells (Figures 4B–4D). This difference indicates that the nonlinearity observed in the On parasol responses originates after the divergence of signals into On and Off circuits. At low light levels, this divergence occurs late in the circuitry at the level of the AII amacrine cell output (Figure 4A). As a consequence, we would expect a nonlinear mechanism shaping AII amacrine responses to affect both On and Off parasol cell responses. Since Off parasol responses were linear, this makes the On cone bipolar output synapse a likely location for the nonlinearity.

Second, the nonlinearity affected both rod and cone signals. At low light levels, rod and cone signals traverse the retina through distinct circuitry until they reach the cone bipolar synaptic terminal (Figure 4E). Thus rod- and cone-mediated excitatory synaptic inputs to an On parasol ganglion cell should share the same nonlinearity if it is indeed located at this synapse; they are unlikely to share the same nonlinearity if it is located at a different site in the rod bipolar circuitry.

The difference in spectral sensitivity between rods and long-wavelength-sensitive cones allowed separation of rod- and cone-mediated responses in the ganglion cell inputs [28]. Responses to long-wavelength flashes had a fast cone-mediated component and a slower rod-mediated component (purple trace in Figure 4F), whereas responses to short-wavelength flashes (blue trace in Figure 4F) had only the slow (rod) component. Rod-mediated responses in these experiments were quite strong and often exhibited oscillations during

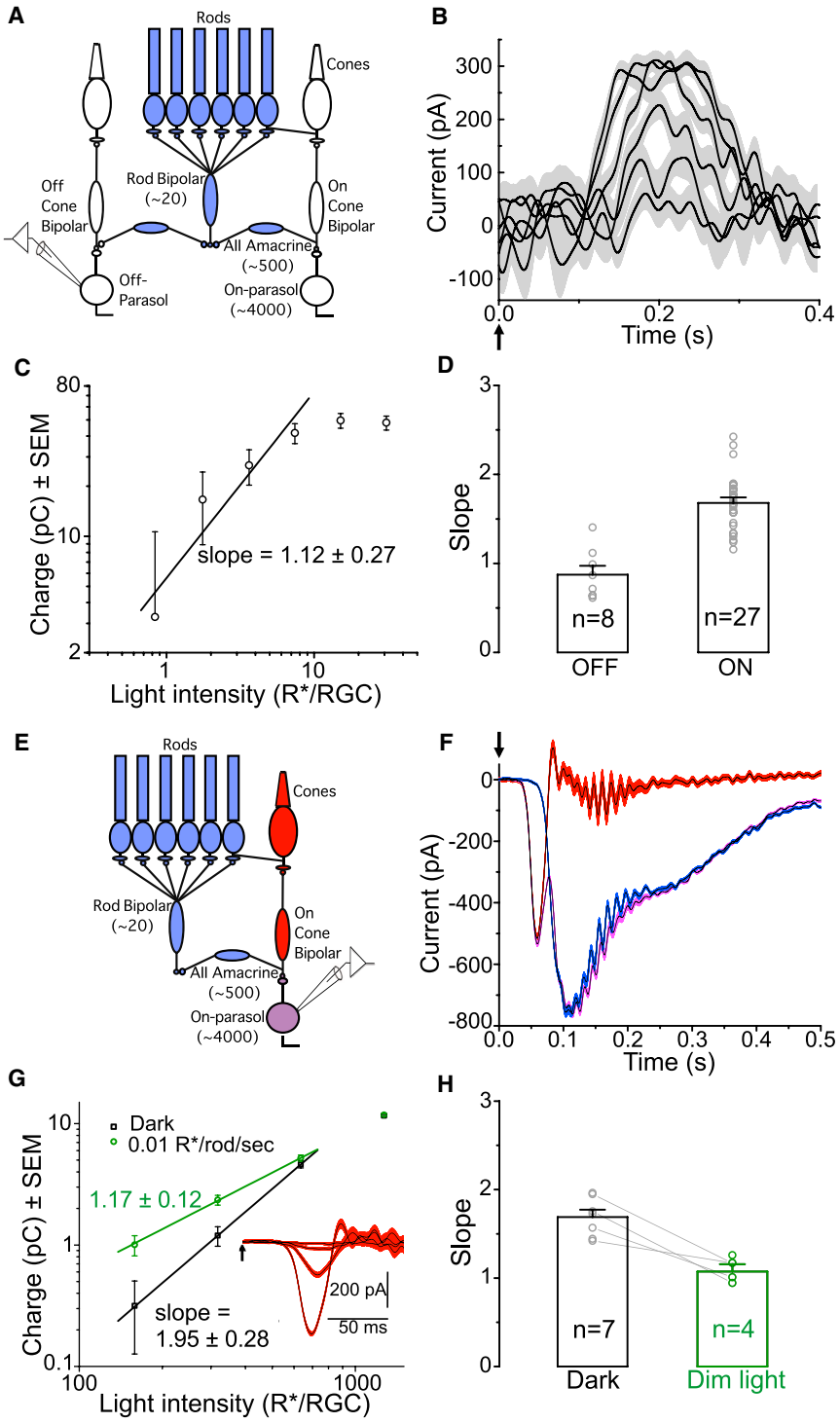

Figure 4. The Thresholding Nonlinearity Is Located at the Synapse of the On Cone Bipolar onto the On Parasol Cell

(A–D) Nonlinearity is not part of the Off-parasol circuit, which shares with the On parasol circuit the stages up to the AII amacrine cell, as indicated by blue shading in the diagram in (A). Rod convergence at different levels of the circuit is shown in parentheses. Excitatory synaptic inputs to an Off parasol cell elicited by the same flash strengths as used to probe On and Off parasol cells as in Figures 1 and 2 (black, mean; gray, SEM; n = 21 traces) are shown in (B). The traces plot the decrease elicited by a flash in tonic excitation in darkness (such that the strongest two flashes completely abolish tonic excitation similarly as they completely abolish spiking activity in the Off parasol shown in Figures 1B and 1D). Stimulus-response relation for Off parasol inputs is shown in (C). Collected data comparing slopes of stimulus-response relations for excitatory inputs to On and Off parasol cells are shown in (D). (E–H) Rod- and cone-mediated signals share a common thresholding nonlinearity. Retinal circuits conveying rod and cone signals to an On parasol ganglion cell in the dark are shown in (E). The only shared element is the cone bipolar synaptic terminal onto On parasol. Separation of rod and cone responses is shown in (F). Long-wavelength flashes elicited responses with a fast cone component and a slow rod component. Subtracting from this a pure rod response matching the rod component (elicited by an appropriately chosen short-wavelength flash) allowed isolation of the cone response (the width of each trace indicates ±SEM). Stimulus-response relation for isolated cone responses (inset) in darkness (black) and in the presence of a dim background (green) are shown in (G). Collected data on the slope of the cone stimulus-response relation in the dark and in the presence of the dim background are shown in (H).
See also Figure S1.

recovery (Figure 4F); these are most likely due to strong activation of inner retina feedback circuits.

With the strengths of long- and short-wavelength flashes chosen to elicit rod-mediated responses of equal amplitude, the cone-mediated response could be estimated from the difference between the responses (red trace in Figure 4F). The cone-mediated responses were nonlinear in darkness (slope = 1.68 ± 0.08, mean ± SEM, n = 7; Figure 4G), but became linear (slope = 1.09 ± 0.07, n = 4) in the presence of backgrounds (0.008–0.01 R*/rod/s) that only affected rods (Figures 4G and 4H). Near-identical backgrounds linearized rod-mediated responses (Figures 3A–3D). The similarity in the nonlinearities affecting rod- and cone-mediated responses provides additional evidence for a location at the synapse between On cone bipolar cells and On parasol ganglion cells.

The Effect of Retinal Nonlinearity on Encoding of Sparse Photon Responses

The results above show that Off parasol ganglion cells integrate photon absorptions linearly or near linearly, whereas On parasol cells integrate photon absorptions nonlinearly due to thresholding at the On cone bipolar output synapse. This section describes the consequences of this difference for the encoding of responses to weak light inputs in the retinal output. We explored this issue by constructing a model that allowed manipulation of how single-photon responses are integrated (Figure 5A; see the Experimental Procedures for details).

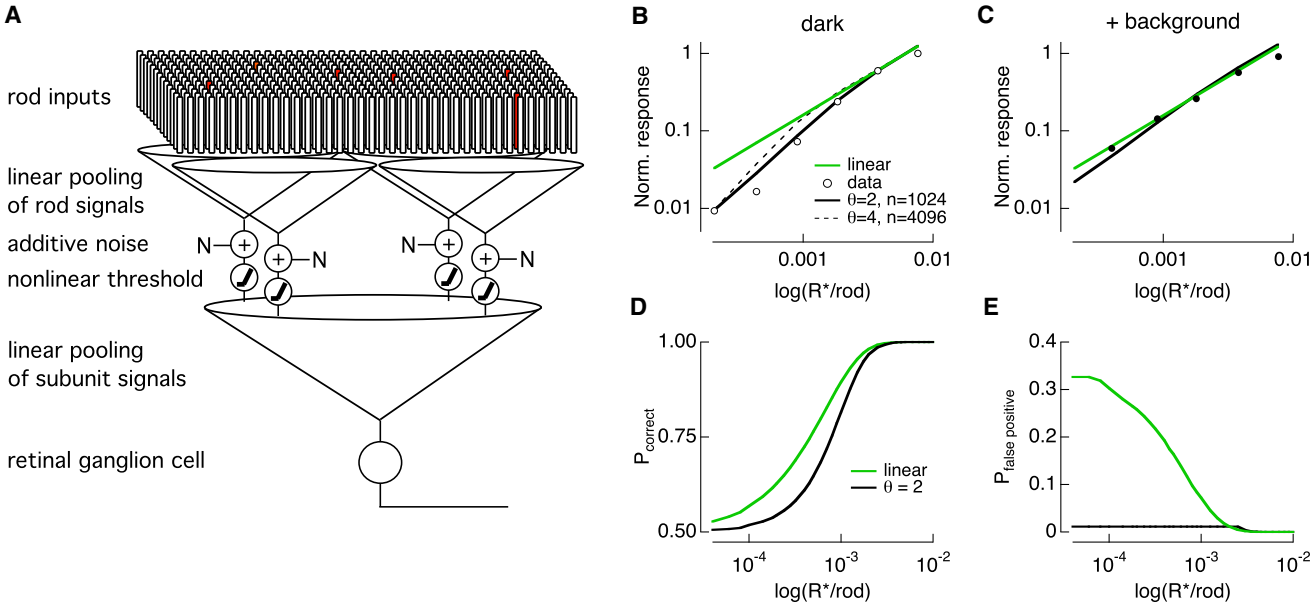

Figure 5. Predicted Impact of the Observed Nonlinearity on Sensitivity of the retinal Output Signals

(A) Schematic of the model. Rod signals arising from single-photon absorptions and spontaneous photon-like noise events in a subset of rods (red) were pooled linearly. Additive synaptic noise (N) was added, and the pooled signals and noise were passed through a nonlinear threshold to represent the inner retinal subunit responses. Multiple subunits were pooled to generate modeled ganglion cell responses.

(B) Stimulus-response relations for models (see the Experimental Procedures) with different thresholds (θ) and subunit sizes (n) compared to data from an example On parasol cell.

(C) Stimulus-response relations for different models in the presence of a background producing 0.008 R*/rod/s. Symbols show the measured stimulus-response relation under background from the same cell as in (B).

(D) Flash/no-flash discrimination performance for an observer of the modeled ganglion cell outputs (θ = 2). The modeled ganglion cell received (indirect) input from 4,096 rods.

(E) False-positive rate across flash strengths for an observer of the modeled ganglion cell outputs.

See also Figure S1.

The distribution of rod responses was modeled assuming a Poisson distribution of absorbed photons with a mean determined by the flash strength and a rate of spontaneous photon-like noise events of 0.0037 per rod per second [5]. Photon-like noise events were weighted according to when they occurred relative to the flash. We measured the temporal integration properties of the nonlinearity by delivering pairs of dim flashes, each producing ~2 R*/RGC, while measuring excitatory synaptic inputs to an On parasol cell (Figure 6A). At this flash strength, responses to individual photon absorptions are integrated nonlinearly (Figure 2A). To measure the time course of these nonlinear interactions, we subtracted the response to the initial flash (thick trace in Figure 6A) from the responses to the paired flashes (thin traces in Figure 6A). The isolated responses to the second flash (Figure 6B) showed clear nonlinear potentiation at short time offsets before declining to a steady amplitude for longer time offsets. We quantified the nonlinear interactions using an interaction index, defined as the integral of the average isolated response to the second flash of the pair divided by the integral of the average response to a single flash delivered alone. Collected across cells, the strength of nonlinear paired-flash interactions declined approximately exponentially with a 50 ms time constant (Figure 6C). The distribution of amplitudes of spontaneous noise events and background photon absorptions (for models that included background light) were constructed using this exponential weighting over time.

Given this description of the relevant signals in the rod array, we next modeled nonlinear subunits. Responses from a collection of rods were summed linearly, and Gaussian noise was added to account for cellular and synaptic noise introduced within the retinal circuitry. The level of added Gaussian noise was chosen to replicate the 20-fold reduction in noise produced by the nonlinearity (Figure 3D). This pooled signal was subjected to a nonlinear threshold that eliminated responses smaller than the threshold and retained those exceeding it. This threshold captures nonlinear interactions between signals in different rods—including between photon-like noise events and events from real photon absorptions. Responses from several such nonlinear subunits were combined to account for the 4,096 (2^{12}; see the Experimental Procedures) rods providing input to the modeled ganglion cell (e.g., if the subunits contained 1,024 rods, four subunits were added).

We varied the threshold and the number of rods in each subunit to identify conditions that approximated those observed experimentally. Models with 1,024 rods per subunit and a threshold of two photon-like events captured both the nonlinear dependence of response amplitude on flash strength and the relief of this nonlinearity by weak backgrounds (Figures 5B and 5C). Thresholds substantially lower than two failed to capture the nonlinearity as they rejected too few single-photon responses and hence produced a too-linear stimulus-response relation. Thresholds substantially higher than three produced a too-steep stimulus-response relation and required levels of rod convergence greater than the known anatomical convergence within the rod bipolar circuit (Figure 5B), assuming that the convergence in primate is similar to that in cats [26].

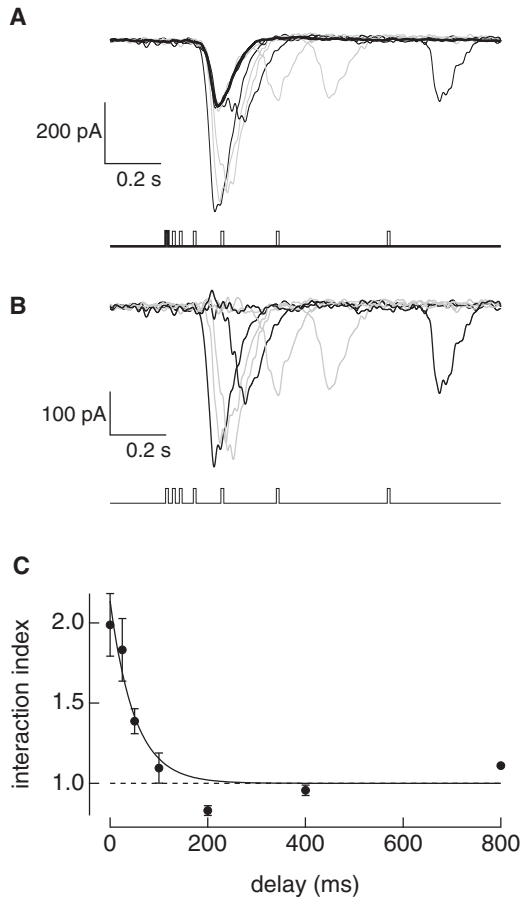

Figure 6. Measurement of the Time Window for Nonlinear Interactions in On Parasol Cells

(A) Excitatory synaptic currents elicited by a single flash (thick trace) or pairs of flashes delivered at different time offsets.

(B) Responses to the second flash of a pair with the response to the first flash subtracted.

(C) Interaction index, defined as the area of subtracted response in (B) divided by the area of the response to a single flash from (A). Each point represents the mean ± SEM across five cells. The smooth line is an exponential with a 50 ms time constant.

We used this model to compare detection thresholds of linear (e.g., Off parasol) and nonlinear (e.g., On parasol) models using two-alternative forced-choice discrimination of flash versus no-flash responses. Because the model predicts full response distributions, we could use a simple maximum-likelihood procedure for discrimination. Thus, at a given flash strength, each possible response amplitude was classified as more likely to correspond to a trial with a flash or with no flash; weighting these classification signals by the probability of each response amplitude and summing determined the probability of correct discrimination (see the Experimental Procedures). The nonlinearity shifted the relationship between probability correct and flash strength to the right, such that the flash identified correctly on 75% of the trials increased in strength by ~40% compared to a linear model (Figure 5D). This decreased sensitivity is most prominent at the lowest flash strengths, consistent with direct discrimination based on the measured ganglion cell responses (Figure 1E). At the lowest flash strengths, subunits in the model rarely received more than one photon and the threshold decreased signal more than it decreased noise (see also Figure 3E).

We also monitored false-positive responses—i.e., responses during trials in which no flash was delivered that were erroneously identified as flash responses. Nonlinear integration decreased the rate of false-positive responses more than 30-fold compared to linear integration (Figure 5E). The decreased false-positive rate is a direct result of the threshold eliminating the added noise arising downstream of rods and noise arising from spontaneous photon-like events in rods. These noise sources, if not eliminated, cause noise in the modeled ganglion cell responses to often mimic responses to weak flashes and create false-positive responses. Thus, false negatives (missed photon absorptions) dominate discrimination errors when the rod array is read out nonlinearly, whereas false positives are much more prominent when the readout is linear (see also Figure 1E).

The model shows directly the impact of the nonlinearity on the balance between false-positive responses and sensitivity. Because the nonlinearity limits information about single-photon absorptions available to the brain, it constrains the ability to trade false-positive responses for improved detection of weak inputs. At the same time, the nonlinearity makes extracting information about incident photons from the On parasol output signals exceedingly simple since so little noise remains in the responses.

Discussion

We characterized the responses of primate On and Off parasol ganglion cells to single-photon absorptions in the rod photoreceptors. Our results show a fundamental difference in how single-photon responses generated in the rods are read out by the circuits controlling responses of On and Off parasol ganglion cells. On parasol cell responses are shaped by a previously unappreciated nonlinear processing step located at the excitatory synapse between On cone bipolar cells and On parasol ganglion cells. Off parasol cells do not share this nonlinearity. The nonlinearity causes On parasol cells to provide a thresholded and remarkably noise-free estimate of the incoming photon stream, but it also eliminates responses to many single-photon absorptions. These findings require revisiting long-held ideas about how responses near absolute visual threshold are encoded in the retinal output.

Retinal Strategy in Sparse Signal Detection

Many neural circuits face the challenge of integrating noisy inputs under conditions in which the signal of interest is sparse. Indeed, this problem recurs as signals traverse the retina through the rod bipolar circuitry and as elements of this circuitry necessarily add noise to the sparse responses to single photons. Retinal circuits, interestingly, do not adopt a single approach to coding under these conditions.

Readout noise in near-threshold detection tasks can often be mitigated by strongly amplifying signals in the sensory receptors themselves and then averaging over receptors to improve the signal-to-noise ratio. These strategies are of limited effectiveness, however, when signals are sparse; in particular, if noise is present in all receptors and signals are carried by less than the square root of the number of receptors, averaging will decrease rather than increase the signal-to-noise ratio. These are precisely the conditions under which rod vision operates at visual threshold, and hence other approaches are needed to account for absolute visual sensitivity.

Previous work indicates that a nonlinearity at the synapse between rods and rod bipolar cells serves to substantially improve the sensitivity of rod-mediated responses by eliminating much of the noise in rod phototransduction [8–10]. Because noise fluctuations and single-photon responses cannot be unambiguously distinguished, this thresholding necessarily also eliminates a sizable fraction of the single-photon responses. Indeed, the position of the threshold agrees well with predictions based on retaining responses more likely to be signal than noise. This synapse provides a universal first step in the processing of rod signals under conditions where the rod bipolar pathway is the dominant conduit of signals across the retina.

Synaptic and cellular processing steps after the rod bipolar synapse inevitably add noise to rod-mediated signals. This added noise means that later stages of retinal processing provide additional opportunities to reject noise at the cost of rejecting small signals. Here we show that different outputs of the primate retina differ in noise level and retention of single-photon responses. Responses of On parasol cells were consistent with a coincidence detection model incorporating a threshold; thresholding occurred at the synapse between On cone bipolar cells and On parasol cells. Off parasol cells instead integrated single-photon responses linearly or near linearly. Both cell types shared similar sensitivity to flashes near absolute visual threshold. Thus, the initial nonlinearity at the synapse between rods and rod bipolar cells provides noise rejection common to all retinal readouts, whereas the nonlinearity at the On cone bipolar output synapse causes On, but not Off, parasol cells to encode a low-noise but thresholded version of the incoming photon stream.

The distinctive strategies On and Off parasol circuits employ are remarkably specific. Mean lights producing less than one absorbed photon per hundred rods per second, only slightly greater than the rate of spontaneous rhodopsin activation in the dark, relieved the nonlinearity in the On parasol circuits and caused them to integrate single-photon responses linearly or near linearly. Under these conditions, responses of On and Off parasol cells were more symmetrical. This strong dependence on background light highlights the specificity of the thresholding mechanism in the On pathway in the darkness. This thresholding is one of several examples in which fine tuning of a simple synaptic mechanism—in this case the linearity or nonlinearity of the On cone bipolar synaptic output—can have dramatic effects on circuit function (reviewed by [29]).

Comparison with Classical Studies of Absolute Visual Sensitivity

Two models were proposed in the mid-1900s to account for behavioral sensitivity to small, brief flashes [30, 31]. The first model posits that human behavioral sensitivity to dim flashes relies on detecting coincident photons [32]. It was even hypothesized that such coincidence detection might arise from nonlinear subunits in the retina [33]. The second model posits that each rhodopsin activation—whether spontaneous or through photon absorption—modulates the retinal output (reviewed in [5, 17]).

The model in which the retina reports each rhodopsin activation has gained favor, although the experiments supporting it are suggestive rather than definitive. Physiological evidence is largely based on in vivo recordings from On ganglion cells in anesthetized cats [22, 23]. The high dark firing rates in these recordings are consistent with the proposal that each spontaneous rhodopsin activation contributes to the retinal output. This behavior is fundamentally different from that of dark-adapted On parasol ganglion cells in the in vitro primate retina. The difference may arise from species differences and/or differences in recording conditions (in vitro versus in vivo under anesthesia); recordings in matching conditions will be needed to resolve this discrepancy. On ganglion cells in amphibians (toads and frogs [34–36]) and in mice (unpublished data) operate similarly to primate On parasol cells, maintaining a near-zero spontaneous firing rate in the dark; this behavior is more consistent with a thresholding mechanism eliminating noise originating from spontaneous rhodopsin activations. Off ganglion cells in mice, like those reported here, maintain high spontaneous firing rates in the dark [25].

Behavioral evidence that every rhodopsin activation contributes to the retinal output comes from the ability of humans to lower detection threshold at the cost of an increased rate of false-positive responses ([37]; for a review, see [5, 17]). Recent behavioral measurements, however, suggest that the ability to trade false-positive responses for sensitivity falls short of expectations for a noisy detector that responds to every photon [38]. This finding is consistent with a threshold that eliminates a fraction of the single-photon responses. Further refinement of such behavioral experiments could test the impact of the thresholding we observe here.

The differences documented here in how On and Off parasol cells integrate single-photon responses provides an alternative to the classic models used to explain visual perception: the brain has access to retinal outputs that are either nearly noise-free but thresholded (via the On parasol cells) or that are noisy but retain information about each photon absorption (via the Off parasol cells). This result will need to be incorporated into interpretation of psychophysical measures of absolute sensitivity. Specifically, since the brain has access to both linear and nonlinear readouts of the weakest light stimuli, changing the weighting associated with different retinal outputs could contribute to the well-established behavioral ability to trade false-positive responses for sensitivity [5, 39]. Such reweighting of different retinal outputs could similarly allow central circuits to adopt responses consistent with either of the classic models used to account for behavioral sensitivity. Such a general computation strategy has implications far beyond vision.

Experimental Procedures

Electrophysiological Recordings

All recordings were from primate (*Macaca nemestrina* and *fascicularis*) parasol ganglion cells. Recordings were from peripheral retina (eccentricity >30°), except those of Figures 4F–4H, which specifically targeted more central cells (eccentricity 15°–20°) with stronger cone inputs. Primate retina was obtained through the Tissue Distribution Program of the Regional Primate Center at the University of Washington. Retina storage, handling, and recording followed previously published procedures [28, 40]. All experiments were done in accordance with guidelines for the care and use of animals at the University of Washington. The figures are based on recordings at 32°C–34°C; the essential features of the nonlinearity in the On parasol responses were similar at 37°C (for five cells at 37°C, the slope as in Figure 2A was 1.84 ± 0.11, mean ± SEM, and the dark firing rate was 0.8 ± 0.3 Hz).

Light Stimuli

Calibrated light stimuli (10–20 ms flashes and steady background lights, spatially uniform spot, 560 μm in diameter) were delivered from blue and/or green light-emitting diodes (LEDs; peak output at 460 nm and 510 nm) in rod-mediated experiments. A red LED (peak at 640 nm) was used to elicit cone-mediated response components (Figures 4F–4H). LED light output was focused on the retina by the microscope condenser.

Stimulus intensities are given in terms of isomerizations per rod per second (R*/rod/s), based on the measured LED spectral output, rod spectral sensitivity, and an assumed collecting area of 1 μm^2 [41]. We converted light intensities to isomerizations per parasol ganglion cell (R*/RGC) by assuming convergence of 4,000 rods for macaque parasol cells [21].

Solutions

Cell-attached recordings were made using pipettes filled with Ames solution. Whole-cell voltage-clamp recordings were made using pipettes filled with 105 mM $CsCH_3SO_3$, 10 mM TEA-Cl, 20 mM HEPES, 10 mM EGTA, 5 mM Mg-ATP, 0.5 mM Tris-GTP, and 2 mM QX-314 (pH ~7.3 with CsOH; ~280 mOsm). Excitatory synaptic inputs were measured by voltage clamping of cells near the reversal potential for inhibitory inputs (~−70 mV). Reported holding voltages have been corrected for a −10 mV junction potential. Series resistance was typically 6–10 MΩ and was compensated 50%.

Data were collected only from cells that met two criteria. First, prior to mounting of the retina in the recording chamber, attachment to the pigment epithelium had to be excellent. Strong attachment was critical for finding On parasols in their most sensitive state. Second, we required that cells generate an average of four to five spikes in response to a brief flash producing 0.001–0.002 R*/rod. These criteria were established on the assumption that the most sensitive cells we record from in vitro resemble those in vivo.

Two-Interval Forced-Choice Discrimination Task

To discriminate flash and no-flash experimental trials as in Figure 1, we computed the instantaneous firing rate of the ganglion cell in 10 ms time bins. The mean response across all flash strengths was used as the discriminant. The trial to be discriminated was not used to calculate the discriminant to remove a possible source of bias. For each trial, we computed the correlations between the discriminant and the 500 ms intervals preceding and following the 10–20 ms flash. We classified the flash detection as correct if the correlation with response after the flash was larger than that with the response prior to the flash. If the correlation values were equal, half of the epochs were assigned as correct choices and half as incorrect choices corresponding to the forced-choice procedure. The general procedure is in line with previous literature [24, 25].

Retinal Circuit Model

Figure 5 is based on a model for the parasol responses. For a given flash strength, rod signals were approximated by sampling from a Poisson distribution corresponding to the mean number of absorbed photons produced by the flash. Noise from spontaneous rhodopsin activation was added, assuming a rate of 0.0037 events/rod/s [5] and an exponential weighting function with a time constant of 50 ms (see Figure 6). Background photons, when present, were treated identically. Thus, the distribution of spontaneous and background events was obtained from the probability of an event occurring at a given time offset relative to the flash multiplied by the exponential weighting function at that time. This distribution was convolved with the Poisson distribution describing photon absorptions from the flash.

For modeling of nonlinearities at different circuit locations, signals from a collection of rods (constrained to be a power of 2 for computational efficiency) were pooled to create a nonlinear "subunit" of the parasol cell receptive field, stimulus-independent Gaussian noise was added to the pooled rod signal to approximate synaptic noise, and the resulting signals were thresholded to model the observed nonlinearity (Figure 5A). Outputs of several such nonlinear subunits were summed to predict responses of a ganglion cell receiving (indirect) input from 4,096 rods. The combination of noise amplitude and threshold was constrained such that the threshold reduced the variance of the pooled rod signals by a factor of ~20 (to match the data from the On parasol cell in Figure 5 and the collected data in Figure 3D). The combination of subunit size and threshold determined the shape of the stimulus-response relation, with thresholds of near two and subunit sizes near 1,000 rods providing the best match to the data (Figure 5B). Models with thresholds of four or more fit the data poorly and required subunits containing at least 4,000 rods; this high level of convergence is inconsistent with the known anatomy, assuming that primates and cats are similar [26]. The model did not incorporate rejection of single-photon responses at the synapse between rods and rod bipolar cells [8] (Figure S1); including this step would increase the level of convergence required to fit the data by at most by a factor of two (if at most half of the single photon responses are rejected). This increase in convergence would not change the central conclusion of the modeling that a threshold of two to three photon-like events is required to fit the data.

The impact of nonlinear integration on behavioral sensitivity was explored in the context of a two-alternative forced-choice procedure in which the task was to determine whether a single response was produced by a flash or not. Discrimination used full distributions of response amplitudes. Thus, the model predicts, at a given flash strength, the probability that a given response amplitude A was produced on a no-flash trial [$P_{NF}(A)$] and on a flash trial [$P_F(A)$]. Amplitudes were classified as more likely corresponding to a flash or no-flash trial from the ratio of the probabilities. This procedure produced a discrimination criterion for every A. Correct discrimination, as in Figure 5D, was determined by summing $P_F(A)$ at all amplitudes A more likely to correspond to flashes [i.e., where $P_F(A) > P_{NF}(A)$]. False positives, as in Figure 5E, were determined by summing $P_{NF}(A)$ at the same amplitudes.

Supplemental Information

Supplemental Information includes one figure and can be found with this article online at http://dx.doi.org/10.1016/j.cub.2014.10.028.

Author Contributions

P.A.-L. and F.R. designed experiments, collected and analyzed data, and wrote the paper.

Acknowledgments

We thank Kristian Donner, Greg Field, Greg Horwitz, and Greg Schwartz for helpful comments on the manuscript and Paul Newman, Eric Martinson, and Mark Cafaro for excellent technical assistance. Support was provided by the HHMI (F.R.), NIH (EY11850 to F.R.), Academy of Finland (253314, 256156 to P.A.-L.), Sigrid Jusélius Foundation (P.A.-L.), and Emil Aaltonen Foundation (P.A.-L.).

Received: September 14, 2014
Revised: October 9, 2014
Accepted: October 9, 2014
Published: November 6, 2014

References

1. Crawford, A.C., and Fettiplace, R. (1985). The mechanical properties of ciliary bundles of turtle cochlear hair cells. J. Physiol. *364*, 359–379.
2. Hudspeth, A.J. (1989). How the ear's works work. Nature *341*, 397–404.
3. Leinders-Zufall, T., Lane, A.P., Puche, A.C., Ma, W., Novotny, M.V., Shipley, M.T., and Zufall, F. (2000). Ultrasensitive pheromone detection by mammalian vomeronasal neurons. Nature *405*, 792–796.
4. Baylor, D.A., Lamb, T.D., and Yau, K.W. (1979). Responses of retinal rods to single photons. J. Physiol. *288*, 613–634.
5. Field, G.D., Sampath, A.P., and Rieke, F. (2005). Retinal processing near absolute threshold: from behavior to mechanism. Annu. Rev. Physiol. *67*, 491–514.
6. Baylor, D.A., Nunn, B.J., and Schnapf, J.L. (1984). The photocurrent, noise and spectral sensitivity of rods of the monkey Macaca fascicularis. J. Physiol. *357*, 575–607.
7. van Rossum, M.C., and Smith, R.G. (1998). Noise removal at the rod synapse of mammalian retina. Vis. Neurosci. *15*, 809–821.
8. Field, G.D., and Rieke, F. (2002). Nonlinear signal transfer from mouse rods to bipolar cells and implications for visual sensitivity. Neuron *34*, 773–785.
9. Berntson, A., Smith, R.G., and Taylor, W.R. (2004). Transmission of single photon signals through a binary synapse in the mammalian retina. Vis. Neurosci. *21*, 693–702.
10. Sampath, A.P., and Rieke, F. (2004). Selective transmission of single photon responses by saturation at the rod-to-rod bipolar synapse. Neuron *41*, 431–443.
11. Kolb, H., and Famiglietti, E.V. (1974). Rod and cone pathways in the inner plexiform layer of cat retina. Science *186*, 47–49.
12. Dacheux, R.F., and Raviola, E. (1986). The rod pathway in the rabbit retina: a depolarizing bipolar and amacrine cell. J. Neurosci. *6*, 331–345.
13. Smith, R.G., Freed, M.A., and Sterling, P. (1986). Microcircuitry of the dark-adapted cat retina: functional architecture of the rod-cone network. J. Neurosci. *6*, 3505–3517.
14. Strettoi, E., Dacheux, R.F., and Raviola, E. (1990). Synaptic connections of rod bipolar cells in the inner plexiform layer of the rabbit retina. J. Comp. Neurol. *295*, 449–466.

15. Vaney, D.I., Young, H.M., and Gynther, I.C. (1991). The rod circuit in the rabbit retina. Vis. Neurosci. *7*, 141–154.
16. Wässle, H., Yamashita, M., Greferath, U., Grünert, U., and Müller, F. (1991). The rod bipolar cell of the mammalian retina. Vis. Neurosci. *7*, 99–112.
17. Donner, K. (1992). Noise and the absolute thresholds of cone and rod vision. Vision Res. *32*, 853–866.
18. Purpura, K., Kaplan, E., and Shapley, R.M. (1988). Background light and the contrast gain of primate P and M retinal ganglion cells. Proc. Natl. Acad. Sci. USA *85*, 4534–4537.
19. Field, G.D., Greschner, M., Gauthier, J.L., Rangel, C., Shlens, J., Sher, A., Marshak, D.W., Litke, A.M., and Chichilnisky, E.J. (2009). High-sensitivity rod photoreceptor input to the blue-yellow color opponent pathway in macaque retina. Nat. Neurosci. *12*, 1159–1164.
20. Kaplan, E., and Shapley, R.M. (1982). X and Y cells in the lateral geniculate nucleus of macaque monkeys. J. Physiol. *330*, 125–143.
21. Goodchild, A.K., Ghosh, K.K., and Martin, P.R. (1996). Comparison of photoreceptor spatial density and ganglion cell morphology in the retina of human, macaque monkey, cat, and the marmoset Callithrix jacchus. J. Comp. Neurol. *366*, 55–75.
22. Barlow, H.B., Levick, W.R., and Yoon, M. (1971). Responses to single quanta of light in retinal ganglion cells of the cat. Vision Res. *3* (*Suppl 3*), 87–101.
23. Mastronarde, D.N. (1983). Correlated firing of cat retinal ganglion cells. II. Responses of X- and Y-cells to single quantal events. J. Neurophysiol. *49*, 325–349.
24. Chichilnisky, E.J., and Rieke, F. (2005). Detection sensitivity and temporal resolution of visual signals near absolute threshold in the salamander retina. J. Neurosci. *25*, 318–330.
25. Murphy, G.J., and Rieke, F. (2011). Electrical synaptic input to ganglion cells underlies differences in the output and absolute sensitivity of parallel retinal circuits. J. Neurosci. *31*, 12218–12228.
26. Sterling, P., Freed, M.A., and Smith, R.G. (1988). Architecture of rod and cone circuits to the on-beta ganglion cell. J. Neurosci. *8*, 623–642.
27. Vardi, N., and Smith, R.G. (1996). The AII amacrine network: coupling can increase correlated activity. Vision Res. *36*, 3743–3757.
28. Dunn, F.A., Lankheet, M.J., and Rieke, F. (2007). Light adaptation in cone vision involves switching between receptor and post-receptor sites. Nature *449*, 603–606.
29. Gollisch, T., and Meister, M. (2010). Eye smarter than scientists believed: neural computations in circuits of the retina. Neuron *65*, 150–164.
30. Hecht, S., Shlaer, S., and Pirenne, M.H. (1942). Energy, quanta, and vision. J. Gen. Physiol. *25*, 819–840.
31. Van Der Velden, H.A. (1946). The number of quanta necessary for the perception of light of the human eye. Ophthalmologica *111*, 321–331.
32. Bouman, M.A., and Van Der Velden, H.A. (1947). The two-quanta explanation of the dependence of the threshold values and visual acuity on the visual angle and the time of observation. J. Opt. Soc. Am. *37*, 908–919.
33. Pirenne, M.H. (1948). Independent light-detectors in the peripheral retina. J. Physiol. *107*, 47.
34. Reuter, T., Donner, K., and Copenhagen, D.R. (1986). Does the random distribution of discrete photoreceptor events limit the sensitivity of the retina? Neurosci. Res. Suppl. *4*, S163–S180.
35. Donner, K. (1989). The absolute sensitivity of vision: can a frog become a perfect detector of light-induced and dark rod events? Phys. Scr. *39*, 133–140.
36. Donner, K., Copenhagen, D.R., and Reuter, T. (1990). Weber and noise adaptation in the retina of the toad Bufo marinus. J. Gen. Physiol. *95*, 733–753.
37. Sakitt, B. (1972). Counting every quantum. J. Physiol. *223*, 131–150.
38. Koenig, D., and Hofer, H. (2011). The absolute threshold of cone vision. J. Vis. *11*, 1–24.
39. Barlow, H.B. (1956). Retinal noise and absolute threshold. J. Opt. Soc. Am. *46*, 634–639.
40. Ala-Laurila, P., Greschner, M., Chichilnisky, E.J., and Rieke, F. (2011). Cone photoreceptor contributions to noise and correlations in the retinal output. Nat. Neurosci. *14*, 1309–1316.
41. Schneeweis, D.M., and Schnapf, J.L. (1995). Photovoltage of rods and cones in the macaque retina. Science *268*, 1053–1056.